Interfacial Rheology of Coexisting Solid and Fluid Monolayers

A. K. Sachan[1], **S. Q. Choi**[2], **K.H. Kim**[2], **Q. Tang**[1], **L. Hwang**[3], **K. Y.C. Lee**[3], **T. M. Squires**[4], and **J. A. Zasadzinski**[*,1]

[1]Department of Chemical Engineering and Materials Science, University of Minnesota, Minneapolis, Minnesota 55455

[2]Departments of Chemical and Biomolecular Engineering and KINC, KAIST, Daejeon, 305-701, Korea

[3]Department of Chemistry, Institute for Biophysical Dynamics, and James Franck Institute, University of Chicago, Chicago, Illinois 60637

[4]Department of Chemical Engineering, University of California, Santa Barbara, Ca 93106

Abstract

Biologically relevant monolayer and bilayer films often consist of micron-scale high viscosity domains in a continuous low viscosity matrix. Here we show that this morphology can cause the overall monolayer fluidity to vary by orders of magnitude over a limited range of monolayer composition. Modeling the system as a two-dimensional suspension in analogy to classic three-dimensional suspensions of hard spheres in a liquid solvent explains the rheological data with no adjustable parameters. In monolayers with ordered, highly viscous domains dispersed in a continuous low viscosity matrix, the surface viscosity increases as a power law with the area fraction of viscous domains. Changing the phase of the continuous matrix from a disordered fluid phase to a more ordered, condensed phase dramatically changes the overall monolayer viscosity. Small changes in the domain density and/or continuous matrix composition can alter themonolayerviscosity by orders of magnitude.

Keywords

Lipid domains; lung surfactants; interfacial rheology; hard sphere suspension models

1. Introduction

Two-dimensional phase separation and domain formation play an essential role in the morphology and dynamics of monolayer and bilayer films, and are essential to their physiological function (1-18). In particular, all mammals have a lipid-protein monolayer of lung surfactant that lines the lung alveoli to minimize surface tension during breathing.

Deficiency or disruption of this monolayer leads to potentially fatal respiratory distress syndromes in infants and adults (19, 20). In lung surfactant monolayers, semi-crystalline "solid" phase domains are dispersed in a continuous, lower viscosity matrix, which may be important to maintaining the proper dynamic surface tension needed to facilitate breathing (9-13). In cell membranes, 10 – 1000 nanometer, highly viscous "rafts" distributed in a low viscosity continuous matrix act as transient organizing sites for membrane protein localization and promote coordinated protein function (7, 8). However, how dispersions of viscous domains in a low viscosity matrix affect the overall fluidity of two-dimensional films has not been addressed in much detail (2, 3, 14-18).

While numerous phase diagrams are available that show coexisting immiscible liquid ordered-liquid disordered systems for both monolayers and bilayers (21-38), there are surprisingly few phase diagrams showing coexistence of two liquid condensed (LC), or semi-crystalline ordered phases, or transitions between ordered phases with temperature or surface pressure (39-42). This is likely due to the absence of fluorescent probes that selectively label liquid condensed or solid phases, which makes identifying the composition or even the existence of the two phases difficult. Here we show that grazing incidence X-ray diffraction and surface rheology can give estimates of the composition of coexisting liquid condensed phases that cannot be easily resolved using conventional fluorescence microscopy (2, 4-6, 9, 11-13, 43-47).

We find that ternarymonolayers of dipalmitoylphosphatidylcholine (DPPC), palmitic acid (PA) and dihydrocholesterol (Chol) (48) phase separate into a DPPC-PA rich, tilted liquid condensed (TC) phase and a DPPC-Chol rich liquid expanded (LE) phase at low surface pressures. The DPPC-Chol LE phase transforms to a TC phase at higher surface pressures (~ 12 mN/m) as indicated by the evolution of a chiralmonolayer morphology and a dramatic decrease in the rate of change of surface viscosity with surface pressure. The surface viscosity changes by more than 4 orders of magnitude as the area fraction of the high viscosity DPPC-PA domains is varied, or the DPPC-Cholcontinuous matrix viscosity changes as the dihydrocholesterol fraction is increased.

The measured surface rheology is consistent with a two-dimensional suspension model inspired bymodels of three-dimensional hard sphere suspensions in a fluid solvent (49). Our model and the data show that the overall monolayer viscosity, η_s, increases as a power law in the dispersed DPPC-PA domain area fraction, A: $\eta_s/\eta_{so} = [1 - A/A_c]^{-2}$, in which A_c is the limiting area fraction for 2-D random close packing (50) and η_{so} is the shear viscosity of the continuous DPPC-Chol matrix. At low surface pressure (< 12 mN/m) the continuous matrix is in the liquid expanded (LE) phase, η_{so} is independent of the monolayer composition, and η_s depends only on the DPPC-PA domain area fraction (9, 12). However, at higher surface pressures, the continuous DPPC-Chol matrix transitions to a second tilted condensed (TC) phase, and η_{so} strongly depends on the Chol mole fraction, as does the overall monolayer viscosity, η_s. This mechanism provides a rationale for the dramatic variation in the overall monolayer fluidity due to the domain area fraction and the composition and phase behavior of the continuous matrix.

2. Materials and Methods

2.1 Materials

1,2-dipalmitoyl-sn-glycero-3-phosphocholine (DPPC, R-enantiomer), palmitic acid (PA) and dihydrocholesterol (Chol) (Avanti, Alabaster, AL) with 0.1 wt% Texas-Red DHPE (N-(Texas Red sulfonyl) -1,2-dihexadecanoyl-sn-glycero-3-phosphoethanolamine, Invitrogen, Grand Island, NY) were mixed in the appropriate ratios and diluted to ~0.2 mg/ml in HPLC-grade chloroform (Fisher Scientific, St. Louis, MO) to form a spreading solution. Dihydrocholesterol was used instead of cholesterol to minimize oxidation, but the phase behaviorand domain formationis similar to cholesterol (51). The spreading solution was deposited dropwise onto the clean air-water interface from a Hamilton syringe (Reno, Nevada). 20 minutes were allowed for solvent evaporation prior to film compression. A Milli-Q Gradient A10 system (Millipore, Billerica, MA) provided ultrapure water with a resistivity of at least 18.0 MΩ·cm.

2.2 Isotherms

Isotherms were performed in a Teflon Langmuir trough of our design with a continuous stainless steel ribbon barrier to minimize leakage. Surface pressure (i.e., the reduction in surface tension of a clean air-water interface, γ = 72 mN/m at 25 °C) was measured using a filter paper Wilhelmy plate tensiometer (Riegler and Kirstein, Germany). Interfacial temperature was measured with a miniature infrared thermocouple (Omega Engineering, Stamford, CT) and controlled to 23 ± 1 °C via a circulating water bath. A computer interface written in LabVIEW 9.0 (National Instruments, Austin, TX) handled all aspects of trough control and data collection.

2.3 Fluorescence Imaging

We used a C1 confocal scan head fitted on a Nikon Eclipse 80i upright microscope (Nikon Instruments, Melville, NY) with a Nikon plan apochromatic 20× air immersion objective. The continuous, fluid lipid phase appears bright red in images due to the preferential segregation of the Texas Red dye, while the better ordered domains exclude the dye molecules and appear black (51).

2.3 Grazing Incidence X-ray Diffraction (GIXD)

Two-dimensional GIXD experiments were carried out at the ChemMatCARS station at beam line 15-ID at the Advanced Photon Source, Argonne National Laboratory (52). The desired mixture in chloroform was spread dropwise onto the air/deionized water interface in a custom Langmuir trough, which was temperature-controlled at 23 ± 1 °C. After waiting ~ 30 minutes for solvent evaporation, the monolayers were compressed to the desired surface pressure and annealed for an additional 30 minutes. The trough was enclosed in a helium-filled chamber and the oxygen level was constantly monitored during exposure to the X-ray beam to minimize chemical degradation. The analysis of GIXD data for two-dimensional films at the air-water interface follows that of Kagener et al (53). It is well established that the Bragg peaks correspond to ordering within the alkane chains of the lipid tail groups (54). From the peak values of the reflections, q_{ij}, the real space lattice dimensions are $d_{tj} = 2\pi/q_{ij}$.

2.4 Interfacial Microrheology

Circular ferromagnetic probes (microbuttons) of diameter 100 um, thickness 1 μm, with "button holes" of diameter 3.5 μm were fabricated by photolithography (11, 55), followed by an electron-beam evaporated layer of nickel on one side, followed by a 10 nm layer of gold. The entire wafer was dipped into a 1.0 mM solution of perfluorooctanethiol (Sigma, St. Louis, MO) in ethanol to form a hydrophobic self-assembled monolayer on the gold. A drop of microbuttons in isopropyl alcohol is added to the trough; the microbuttons float to the interface and the hydrophobic surface coating orients them gold side up. The magnetic moments of the microbuttons, $m = (50 \pm 11) \times 10^{-10}$ emu for the 150 nm thick nickel and $(6.9 \pm 2.3) \times 10^{-10}$ emufor the 50 nm thick nickel (11, 13), were calibrated by placing the microbuttons on the water/air interface and measuring the rotational response to a known magnetic field.

A uniform magnetic field of magnitude, B, and orientation, θ, was generated by the output of two independent pairs of electromagnets controlled by a custom LabVIEW code (11, 13) to exert a controlled torque, L, on a microbutton of moment m and orientation ϕ; the direction of the imposed magnetic field was perpendicular to the magnetic moment of the microbutton, so that $L = mB\,[1 \pm (\delta\phi - \delta\theta)^2]$. To measure the frequency-dependent linear viscoelastic response, a sinusoidal magnetic field was applied to generate a time varying applied torque, $mBe^{i\omega t}$. The driving torque was kept small enough that the response was linear, with angular displacements limited to a maximum amplitude, ϑ_0 0.1 rad. The microbutton orientation, $\vartheta_0(\omega)e^{i(\omega t + \gamma)}$, was determined from images of the holes in the microbuttons as a function of applied torque, to determine the rotational resistance,

$$\xi_r^*(\omega) = mBe^{-i\gamma}/i\omega\vartheta_0.$$

The resistance, $\xi_r^*(\omega)$, depends on the Boussinesq number, Bo, which relates interfacial drag to subphase drag. For purely Newtonian monolayers and subphases, Bo is given by $Bo = 2\eta_s/\eta a$, in which a is the microbutton radius, η_s is the surface viscosity and η_s is the subphase viscosity. We find that all of the mixed films are primarily viscous with a Newtonian response over the range of frequency of 0.1 – 5 Hz. For Bo 1, the subphase drag dominates, and the rotational resistance is $\xi_r^*(\omega) = 16/3\eta^* a^3$. For the 100 μm microbuttons used here, the minimum surface viscosity that can be distinguished from the water drag is of order 0.1 μPa-s-m. When $Bo \gg 1$, $\xi_r^*(\omega) = 4\pi\eta_s^* a^2$ and the drag is dominated by the surface viscosity (11). The maximum surface viscosity that can be measured with the microbutton is limited by the magnetic torque that can be applied in our instrument and is ~ 1000 μPa-s-m, which gives us a useful measurement range of about 4 orders of magnitude.

The surface viscosity and elasticity for $Bo \gg 1$ are given by $G'_s = \dfrac{mB}{4\pi a^2\vartheta_0}\cos\gamma$ and

$\eta_s = \dfrac{mB}{4\pi a^2\omega\vartheta_0}\sin\gamma$ as $\eta_s = G''_s/\omega$.

The same exponential dependence of surface viscosity on surface pressure was obtained using 20 and 100 μm microbuttons for a given monolayer suggesting that continuum values of elasticity and viscosity were being measured (9, 11-13). Uncertainties in the measurement of surface viscosity arise due to statistical variations in the magnetic moment, m, of the

microbuttons, the temporal resolution in relating the optical image of the disk to the applied magnetic field, and errors in measuring the phase lag, γ While the 100 μmmicrobuttons are 2 – 10 times larger than the domains observed, the shear field induced by the microbutton motion extends for hundreds of microns containing hundreds of domains. Previousmonolayer rheological results using macroscopic wire rings (10 cm diameter ring, 0.7 mm diameter wires) (44, 56) and 2 mm diameter magnetic needles (2, 3, 43) showed similar trends with surface pressure or area fraction of solid domains (2, 3) and good quantitative agreement for similar monolayers.

3. Results and Discussion

3.1 Monolayer Morphology and Phase Behavior

We used a ternary mixture of dipalmitoylphosphatidylcholine (DPPC), palmitic acid (PA) and dihydrocholesterolas a model system exhibiting high viscosity domains in a continuous low viscosity matrix, over a wide range of surface pressure (Fig. 1). The 3:1 DPPC:PA ratio is also representative of the saturated lipid composition of Survanta and Surfaxin, two commonly used clinical lung surfactants. PA increases the chain ordering of DPPC and induces the formation of rigid, circular, semi-crystalline "tilted condensed" (TC) domains (57, 58) in a continuous background of low viscosity liquid expanded (LE) phase at low surface pressure (Fig. 1). The fluorescent lipid dye (Texas Red DHPE, Invitrogen, Grand Island, NY) is excluded from the ordered domains, which appear black, and is concentrated in the continuous LE phase, which appears red (12) in confocal microscope images. Pure DPPC or DPPC:Chol mixtures are in the LE phase for surface pressures less than ~ 12 mN/m at 23°C (12, 51). As the surface pressure (39) is increased, the area fraction of the black domains increases roughly linearly as shown in Fig. 2 up to ~ 10 – 12 mN/m, and then saturates at a constant value, A_L, at higher surface pressures. For 0 mol% dihydrocholesterol, A_L ~ 0.94; for 0.75 mol%, A_L ~ 0.81 and for 4 mol%, A_L ~ 0.71.The main effect of small mole fractions of dihydrocholesterol is to decrease the area fraction of black domains at a given surface pressure.

However, Fig. 1 shows that at 10 – 13 mN/m, depending on the dihydrocholesterol fraction, spiral "arms" nucleate and grow from the black domains that show a remarkable, uniformly counter-clockwise pattern. As the surface pressure is increased further, the spiral arms grow more dense and tightly wound and eventually fill the space between the original black domains. Figure 3 shows that the morphology of the spiral arms in Fig. 1 is similar to that formed in the TC phase of a binary mixture of DPPC with 2 mol%dihydrocholesterol (12, 37) over the same range of surface pressuresat 23°. Confocal images of the 2 mol% Chol with DPPC monolayer (Fig. 3) show that the spiral arms nucleate from the LE phase (red) at ~10 mN/m atroughly the same surface pressure at which we see the spiral arms nucleate from the black domains in Fig. 1. Cholesterol is known to reduce the line tension between the LE and TC phases of DPPC, causing the domain arms to grow longer and decrease in width with increasing cholesterol fraction (12, 37, 38). Fig. 3 shows that as the surface pressure increases, the arms elongate and spiral into tighter whorls, and eventually fill in the remaining area of the monolayer. At the highest surface pressure, the individual arms cannot be resolved, similar to the continuous phase regions of theternary DPPC:PA:Chol monolayer

above 15 mN/m (Fig. 1). This spiral growth morphology is not as efficient in removing or quenching the Texas-Red DHPE fluorescent lipid, and the red color remains even at high surface pressure, as in the continuous regions of Fig. 1. The similarity between the morphology of the binary DPPC:Cholmonolayer in Fig. 3 and the continuous matrix of the DPPC:PA:Chol mixtures in Fig.1 suggests that the continuous matrix composition is likely enriched in DPPC and dihydrocholesterol relative to the overall monolayer composition. Consistent with our images, vibrational sum frequency generation spectroscopy has shown that the LE phase in 3:1 DPPC:PA mixtures (with no dihydrocholesterol) at 10-12 mN/m (at which the spiral arms begin to nucleate) is nearly pure DPPC (58).

This also suggests that the black domains in Fig. 1 are enriched in palmitic acid relative to the overall monolayer composition. Fig. 4 shows confocal fluorescence images of 5:1, 3:1, 2:1 and 1:1 DPPC:PA monolayers with 4 mol% dihydrocholesterol at $\pi \sim 12$ mN/m. Arms grow from the solid phase domains in all but the 1:1 DPPC:PA monolayer. The area fraction of the black domains increases with decreasing DPPC:PA ratio, suggesting a roughly constant DPPC:PA stoichiometry in the black domains in the 5:1, 3:1 and 2:1 DPPC:PA monolayers. However, for the 1:1 ratio of DPPC:PA, the domains have a different, more rounded shape than at higher DPPC ratios, and no arms grow out of the black domains,. This suggests that the stoichiometry of the black domains is between 1:1 DPPC:PA and 2:1 DPPC:PA.

Fig. 5 shows π-A isotherms of the 5:1, 3:1, 2:1 and 1:1 DPPC:PA ratios, adjusted so that the lift off pressure (59) is at same trough area fraction of 0.8. The 5:1, 3:1 and 2:1 DPPC:PA ratio isotherms have similar features, with a gradual change in slope, (which is proportional to the monolayer compressibility modulus, $K = -A\left(\dfrac{\partial \pi}{\partial A}\right)_T$ (60)), from 10 – 20 mN/m.

The maximum surface pressure that the films can withstand, also known as the collapse pressure, is> 65 mN/m. However, the 1:1 DPPC:PA isotherm has a much greater slope and compressibility modulusat low surface pressures and shows collapse at 52 mN/m, suggestive of a different molecular organization.

3.2 Grazing Incidence X-ray Diffraction

To estimate the composition of the black domains, grazing incidence X-ray diffraction (Fig. 6A) shows that at 10 mN/m, before the spiral arms begin to grow, the diffraction patterns for 3:1 and 2:1 DPPC:PA ratios have peaks at similar spacing, but that 1:1 is significantly different. We assign the Bragg peaks for the three compositions in Fig. 6A at lower q_{xy} to the degenerate (11) and (11) reflections of a distorted hexagonal packing (9, 53, 57); the second peak at higher q_{xy} is due to the non-degenerate (02) reflection. As the (11) reflections were located at $q_z > 0$, and the (02) reflection was centered at $q_z = 0$ (data not shown), the alkane chains are tilted in the nearest neighbor (NN) direction (9, 53). From the peak values of q_{ij} the real space lattice dimensions are $d_{ij} = 2\pi/q_{ij}$. For all three DPPC:PA ratios, the untilted close packed distance between alkane chains is $d_{02} = 4.30 \pm 0.05$ Å. However, d_{11} decreases from $4.6 \pm .05$ Å for the 3:1 and 2:1 DPPC:PA ratios to $4.4 \pm .05$ Å for the 1:1 DPPC:PA ratio, showing that the 1:1 sample has a smaller tilt (9, 53).

Fig. 6B shows GIXD reflections for $\pi > 20$ mN/m; previous work has shown that little change occurs in the peak positions at higher surface pressures (57). There remain two peaks for 3:1 and 2:1 DPPC:PA, but the two peaks at 10 mN/m for the 1:1 DPPC:PA monolayer coalesce into a single broad peak at higher surface pressure. While the 3:1 and 2:1 monolayers have similar distorted hexagonal packings with NN tilt at higher surface pressure, the single peak for the 1:1 sample is consistent with a simple hexagonal packing. For the 3:1 and 2:1 monolayers, $d_{02} = 4.30 \pm 0.05$ Å, and $d_{11} = 4.5 \pm 0.05$ Å. For the 1:1 DPPC:PA monolayer, $d_{02} = d_{11} = 4.23 \pm 0.05$ Å.

From the values of d_{11} and d_{02}, we determine a rectangular two-molecule unit cell of dimensions, $\boldsymbol{a} = d_{10} = [(d_{11})^{-2} - (2d_{02})^{-2}]^{-1/2}$ and $\boldsymbol{b} = 2d_{02} = d_{01}$ (9, 61, 62). The area/alkane chain normal to the interface is $\boldsymbol{ab}/2$. At 10 mN/m, $\boldsymbol{a}$ decreases from 5.4 ± 0.1 for the 3:1 and 2:1 DPPC:PA monolayers (area/chain = 0.23 ± 0.01 nm^2, tilt = 30°), to 5.1 ± 0.1 Å for the 1:1 DPPC:PA monolayer (area/chain = 0.22 ± 0.01 nm^2, tilt = 25°). $\boldsymbol{b} = 8.6 \pm 0.1$ Å for all three monolayers. At the higher surface pressures for the 3:1 and 2:1 DPPC:PA monolayers, $\boldsymbol{a}$ decreases slightly to 5.3 ± 0.1 Å (area/chain = 0.23 ± 0.01 nm^2, tilt = 28°), while $\boldsymbol{b}$ remains 8.6 ± 0.1 Å. For the 1:1 DPPC:PA monolayer at higher surface pressure, $\boldsymbol{a}$ decreases to 4.9 ± 0.1 Å and $\boldsymbol{b} = 8.5 \pm 0.1$ Å (area/chain = 0.21 ± 0.01 nm^2, tilt ~ 0°). For a pure DPPC monolayer at 20 mN/m, $\boldsymbol{a} = 5.8 \pm 0.1$ Å and $\boldsymbol{b} = 8.6 \pm 0.1$ Å (area/chain = 0.25 ± 0.01 nm^2, tilt = 33°)(9).

These unit cell dimensions are consistent with hexagonally close-packing alkane chains (63), which are then tilted to accommodate the excess projected area of the DPPC head group relative to the close-packed chains (53, 57). Tilting the alkane chains occurs without changing the distances between the alkane chains in the plane normal to the chains, which minimizes the energy cost (53, 61, 64). If the tails are assumed to pack with a spacing, a, and the head groups with a spacing, β, then both are satisfied by tilting by an angle θ (with respect to the monolayer normal) such that $\cos\theta = a/\beta$ (61, 64). Tilt in the NN direction causes $\boldsymbol{a}$, which is measured in the plane of the monolayer, to increase. However, $\boldsymbol{b}$ remains constant, as this spacing does not change with tilt if the alkane chains retain their close-packed configuration. PA has a relatively small headgroup area compared to its alkane chain area (61, 64) and by co-crystallizing with DPPC, decreases the effective headgroup spacing, and hence decreases the tilt angle. The similarity in the lattice parameters between the 3:1 and 2:1 DPPC:PA monolayers suggest that the ordered domains have the same ratio of DPPC to PA, which is different than the 1:1 DPPC:PA monolayer, which has significantly different lattice parameters.

One explanation for a limited number of preferred stoichiometric ratios of DPPC to PA is that particular tilt angles may maximize the van der Waals contact (61, 63, 64). In condensed phases, the alkane chains of DPPC and PA are in the *all trans* configuration and have a regular zigzagconformation (61, 64). The zigzag patterns of the alkane chains can nest most closely with another zigzag alkane chain at a limited number of preferred tilts (61, 63, 64), which preserve the close-packing of the chains in the plane perpendicular to the chains. It may be that at certain ratios of DPPC to PA, the effective headgroup spacing, β_e, is such that $\cos\theta_p = a/\beta_e$.

Our results suggest that for the 3:1 DPPC:PA mixtures in Fig. 1, the black domains are a semi-crystalline, tilted condensed (TC) phaseconsisting of DPPC and PA at very similar compositions independent of dihydrocholesterol fraction. PA is depleted in the continuous LE phase as the TC domains grow, which limits the area fraction of black domains to A_L as we see in Fig. 2. At low surface pressures (<12 mN/m) the continuous matrix is a liquid expanded (LE) phase that contains the excess DPPC and likely much of the dihydrocholesterol (16, 57, 58). At 10-13 mN/m, the spiral arms, which consist of a second TC phase composed of the residual DPPC modified by the line-active dihydrocholesterol, nucleate out of the LE phase onto the DPPC:PATC phase domains as in Fig. 3. These spiral arms grow in length and curvature with increasing surface pressure until the continuous phase is completely converted to this DPPC:Chol TC phase. The similarity of the morphology of the DPPC:Chol phase in Fig. 3 to the continuous phase in Fig. 1 is also suggestive that the continuous phase is rich in DPPC-Chol.

3.3 Rheological Response of Two-Phase Monolayers

We find that all of the DPPC:PA:Chol films examined are primarily viscous with a Newtonian response over the range of frequency of 0.1 - 4 Hz. Fig. 7 shows the viscous, G_s'', and elastic, G_s', moduli for a representative monolayer of 3:1 DPPC:PA + 1 mol% dihydrocholesterol at π = 15 mN/m. G_s'' is about an order of magnitude larger than G_s', consistent with the dominant contribution to the disc drag from the monolayer viscosity. We find the slope of the viscous modulus with frequency, ω, over the range of 0.1 – 4 Hz is one within experimental error, consistent with a Newtonian response with a constant viscosity, $\eta_s = G_s''/2\pi\omega$. This response is typical for all of the monolayers measured. At the highest frequency of 5 Hz, both G_s'' and G_s' no longer increase. This is due to the limitation of the microbutton rheometer, which cannot supply sufficient torque to measure monolayers with moduli greater than ~ 2000 μPa-m.

Fig.8 shows the surface shear viscosity of 3:1 DPPC:PA and DPPC monolayers with various mole fractions of dihydrocholesterol (9, 12). The surface viscosity varies by more than four orders of magnitude as a function of surface pressure and monolayer composition. The viscosity exhibits quite different behavior above and below π ~ 12 mN/m, which is the same surface pressure at which the spiral arms nucleate, grow and fill the space between the solid domains (Fig. 1). Below ~ 5 mN/m, the surface viscosity is too low for accurate measurement with our instrument (Bo ~ 1). For $5 < \pi < 12$ mN/m, the viscosity increases exponentially with surface pressure, essentially independent of the dihydrocholesterol fraction. For π>15 mN/m, the slope changes and the viscosity is less dependent on surface pressure, but does depend strongly on the cholesterol fraction. Also plotted in Fig. 8 are the viscosities of mixtures of DPPC with 0, 1.6, and 6.4 mol% dihydrocholesterol (no PA) in the TC phase for π > 15 mN/m (From Ref 12).

What is curious is that the slope of the viscosity vs. surface pressure of the binary DPPC + 1.6 mol% dihydrocholesterol monolayer is virtually identical to the 3:1 DPPC:PA:Chol monolayer with 0.75 mol% dihydrocholesterol, and the slope of the viscosity vs. surface pressure of the binary DPPC monolayer with 6.4 mol% dihydrocholesterol is also quite

similar to the 3:1 DPPC:PA:Chol monolayer with 3 mol% dihydrocholesterol for $\pi > 15$ mN/m. The maximum measurable surface viscosity is <2000 µPa-s-m and is set by the maximum torque that can be applied by the electromagnets onto the microbutton probes. As a result, we cannot measure the surface viscosity of 0 mol% dihydrocholesterol monolayers for surface pressures > 15 mN/m as we cannot apply sufficient torque to move the disc. Dihydrocholesterol causes the surface viscosity to decrease (9, 12) and allow measurements at higher surface pressures.

3.4 The Two-Dimensional Suspension Model

To connect the viscosity to the domain morphology and composition, we use a two-dimensional analog of well-known three dimensional models of hard spheres in a viscous fluid (49, 65); that is, hard circular discs in a continuous low viscosity 2-D matrix (2). In 3-D, hard sphere suspension viscosity scales as the number of particles in contact, divided by the short-time self-diffusivity at the sphere volume fraction, ϕ (49). For non-interacting Brownian spheres, the number of particles in contact scales as $[1 - \phi/\phi_c]^{-1}$ in which ϕ_c is the volume fraction for random close packing. The short time self-diffusivity vanishes as $[1 - \phi/\phi_c]$ because short-ranged, hydrodynamic lubrication forces couple the particles. Hence, the reduced viscosity scales as $\eta/\eta_o = [1 - \phi/\phi_c]^{-2}$ in which η is the steady shear viscosity of the suspension and η_o is the viscosity of the continuous fluid. We speculate that these scaling arguments are equally valid in two dimensions (2), with the area fraction, A, of the high viscosity domains (black in Fig. 1) replacing the sphere volume fraction:

$$\eta_s/\eta_{so} = [1 - A/A_c]^{-2} \quad (1)$$

or

$$\log\eta_s = \log\eta_{so} - 2\log[1 - A/A_c]. \quad (2)$$

η_s is the measured viscosity (Fig. 8) and η_{so} is the viscosity of the continuous matrix.

The choice of the critical area, A_c, to use in the two-dimensional suspension model was based on the limit of "loose random packing" of monodisperse discs without any short or long-range order at the jamming or percolation limit. Hinrichsen et al. find a value of 0.772 ± .002 for the critical area fraction, A_c, with an average coordination number between the discs of 3.5 (50). Disc packings can be compacted to higher area fractions, but this induces long range hexagonal ordering at an order-disorder transition of 0.82 ± .03 (66), which is close to the theoretical limit of $\pi^2/12$.

Fig. 9 shows the surface shear viscosity for the three ternary compositions below 12 mN/m, which is at the break in the slope in Fig. 8, and at the phase transition from LE to TC of the continuous matrix, as can be seen in Fig. 1. Linear regression to Eqn. 2 gives a slope of -2.07 ± 0.13, consistent with the 2-D suspension model. We also determine the intercept, η_{so}=

$0.16 \pm .03$ μPa-s-m, by extrapolating to A=0, which should represent the effective viscosity of the continuous matrix. Over this surface pressure range, the continuous matrix is in the LE phase. There are few literature values of the surface viscosity of LE phases; for dimyristoylphosphatidylethanolamine, our recent measurements using a different rheometer suggests that the LE viscosity is $< 5 \times 10^{-2}$ μPa-s-m (67). Measurements of domain fluctuations for LE phases of DPPC, cholesterol and diphytanoylphosphatidylcholine give an estimated surface viscosity of the LE phase of $\sim 4 \times 10^{-3}$ μPa-s-m (32). For such low values of LE surface viscosity, $Bo \ll 1$ (11, 67) for 100 μm diameter microbuttons on a water subphase. As a result, the apparent surface viscosity of the continuous LE phase from 0 to ~12 mN/m is dominated by the drag from the water subphase and, as such, is independent of the LE phase composition or surface pressure.

For surface pressures > 12 mN/m, there is a distinct break in the slope of the surface viscosity vs surface pressure (Fig. 8) that coincides with the black domain area fraction saturating at A_L (Fig. 1, 2). However, Figs. 1,3 show that the continuous matrix changes from the LE to the TC phase, which increases the continuous matrix viscosity by orders of magnitude depending on the dihydrocholesterol fraction (9, 12, 67). From GIXD, isotherms, and confocal imaging, we can approximate the continuous matrixas a binary mixture of DPPC and dihydrocholesterol. Hence, $\eta_{so}(x, \pi)$ should be similar to that of binary DPPC:Chol monolayers for $\pi > 15$ mN/m (obtained from Ref. 12) with the appropriate fraction of dihydrocholesterol (black symbols in Fig. 8).

To assign the appropriate value for $\eta_{so}(x, \pi)$, we choose the dihydrocholesterol fraction, x, of the available binary mixture viscosities from Ref. 12 to match the rheology data in Fig. 10. For the ternary 3:1 DPPC:PA mixture with 3 mol% dihydrocholesterol, η_s is ~ 20 μPa-s-m at $\pi \sim 12$ mN/m when the solid phase fraction saturates (Fig. 8), which suggests that $\eta_{so}(x, \pi)$ for this mixture is roughly equal to the $\eta_{so} = 0.16$ μPa-s-m we extrapolated for the water drag from our fit to the data in Fig. 9. This value is consistent with a continuous matrix composition of 6.4 mol% dihydrocholesterol in DPPC (Fig. 8). When log $[\eta_{so}(x, \pi)]$ for 6.4 mol% dihydrocholesterol with DPPC is added to -2 log $[1 - A_L/A_C]$ from Fig. 9, the quantitative agreement with the 2-D suspension model is excellent (Fig. 10). This suggests that the dihydrocholesterol is concentrated in the continuous phase by a factor of ~ 2 relative to the nominal monolayer composition.

From Eqn. 2, the difference between the viscosity of two ternary films with the same area fraction of solid phase, A_L, but different continuous matrix dihydrocholesterol fractions x_2 and x_1 is:

$$\log \eta_{s2} - \log \eta_{s1} = \log \eta_{so}(x_2, \pi) - \log \eta_{so}(x_1, \pi) \quad (3)$$

at constant A_L; that is, the difference in Fig. 8 between the log of the viscosity of the ternary DPPC:PA:Cholmixtures should be the same as the difference between the corresponding binary DPPC:Chol mixtures for $\pi > 15$ mN/m. We find that $x_2 \sim 1.6$ mol% dihydrocholesterol in DPPC gives the best fit η_{so} for the ternary DPPC:PA mixture with 0.75

mol% dihydrocholesterol (Fig. 10). Again, the enrichment in dihydrocholesterol of the continuous matrix is roughly 2:1 over the nominal dihydrocholesterol fraction for both 0.75 and 3.0 mol% monolayers. For 0 mol% dihydrocholesterol, we predict that the DPPC:PA surface viscosity is > 1000 μPa-m-s, which is out of the measurement range of our rheometer. However, the absolute values we predict are reasonable, and the slope is similar to the 0.5 mol% dihydrocholesterol monolayer. Fig. 10 shows that both the magnitude and slope of the measured viscosity data are remarkably consistent with the predictions of the 2-D suspension model. The model and our fits to Eqn. 3 provide quantitative estimates of the composition of the continuous matrix. As far as we are aware, there are no other simple methods of estimating the composition of two coexisting liquid condensed phases. For $\pi >$ 12 mN/m, small differences in the dihydrocholesterol fraction of the continuous matrix lead to order of magnitude changes in the overall surface viscosity of the DPPC:PA:Chol, as is the case for the binary DPPC:Chol monolayers (12).

4. Conclusions

Our results show that while the domain morphology of DPPC:PA:Chol mixtures is complicated and beautiful, this model system has the basic elements of "hard discs" in a continuous, lower viscosity matrix. A 2-D suspension model, with $\eta_s/\eta_{so} = [1 - A/A_c]^{-2}$ quantitatively correlates the more than four orders of magnitude variation in surface viscosity. At low surface pressure, the continuous matrix is in the LE phase, and its surface viscosity is sufficiently small that the drag on the discs is provided by the water subphase, and as such, is the same for all monolayers. As the surface pressure increases, the increasing area fraction of the solid phase domains leads to a power law increase in the overall surface viscosity consistent with the two-dimensional suspension model (Eqns. 1, 2). At higher surface pressures, the area fraction of the black domains (Figs. 1, 2) saturates, and the continuous matrix undergoes a phase change to the tilted condensed phase (Figs. 1, 3), which gives a greatly increased viscosity that changes by orders of magnitude depending on the dihydrocholesterol fraction. We are able to estimate that the domains in the DPPC:PA:Chol monolayers are composed of DPPC and PA at a fixed ratio using a combination of monolayer morphology and GIXD (Fig. 4-6), and the continuous phase is a binary DPPC:Chol mixture by comparing the surface viscosity and morphology to that of known binary DPPC:Chol monolayers.

In earlier work, we found that a similar two-dimensional suspension model could be used to correlate the terminal velocity of a two-millimeter diameter magnetic needle when pulled with a constant magnetic force (2) through a phase separated monolayer. Those results were also consistent with $\eta_s/\eta_{so} = [1 - A/A_c]^{-\alpha}$, but showed a better fit with $\alpha = 1$ rather than the current result of $\alpha = 2$. Our current study addresses some of the experimental and modeling limitations of that study that led to this discrepancy. The microbutton rheometer has much greater sensitivity to low values of the surface viscosity than the larger magnetic needle (68).

For a given surface viscosity, the Boussinesq number, $\text{Bo} = \dfrac{2\eta_s}{a\eta}$ for the needle (a ~ 1 mm) was ~ 20 times smaller than that of the 100 μm microbuttons (a ~ 50 μm) used in the current experiments (69). This limits the minimum surface viscosity that can be measured to ~ 1-10 μPa-s-mfor needle instruments (5, 47, 68-71), compared to the ~ 0.1 μPa-s-m with the

microbutton rheometer (9-13, 55). With the microbutton rheometer, we find that the actual range of surface viscosity in these phase-separated systems is four orders of magnitude or more (Fig. 8). Most problematic was the assumption in our previous work that the surface viscosity of the continuous matrix was independent of monolayer composition and surface pressure. Fig. 10 shows that this assumption is incorrect; even small changes in monolayer composition can lead to order of magnitude changes in surface viscosity at high surface pressures.

There are many implications of our results on the design and function of native and clinical lung surfactants. The roles of cholesterol and palmitic acid in LS remain controversial; Survanta and Curosurf have all cholesterol removed; Infasurf contains ~ 7 mol% cholesterol. Palmitic acid (PA) is a product of phospholipase A_2 degradation of DPPC, which may occur during inflammation associated with Acute Respiratory Distress Syndrome or other conditions, butis added to Survanta and the recently approved SurfaxinR, at ~ 3:1 DPPC:PA molar ratio, but not to Curosurf or Infasurf. The consequences of these composition variations are often not apparent from isotherms or other typical LS analysis (12). However, the composition variations in Fig. 8, 10 are similar to the composition variations between Survanta, Surfaxin, Curosurf and Infasurf, and lead to a more than4 order of magnitude variation in surface viscosity. As yet, there is little appreciation of the physiological consequences of the dynamic properties conferred by these concentration and morphology variations. A functional replacement LS must spread quickly to cover the alveolar interfaces during the initial application, and during the rapid increase in alveolar interfacial area during inhalation, suggesting a low surface viscosity may be optimal at low surface pressures. However, at high surface pressure, the surface viscosity or viscoelasticity must be sufficient to resist the Marangoni stresses that arise between the low surface tensions in the deep lung on exhalation and the higher surface tensions in the bronchi and trachea so as to keep the surfactant where it belongs and prevent flow from the alveoli (47). It may be that a large change in surface viscosity with surface pressure is one of the primary physiological requirements for a functional lung surfactant.

Acknowledgments

References and Notes

1. Bringezu F, Ding JQ, Brezesinski G, Zasadzinski JA. Changes in model lung surfactant monolayers induced by palmitic acid. Langmuir. 2001; 17:4641–8.

2. Ding JQ, Warriner HE, Zasadzinski JA. Viscosity of two-dimensional suspensions. Physical Review Letters. 2002; 88:168102. [PubMed: 11955269]

3. Ding JQ, Warriner HE, Zasadzinski JA, Schwartz DK. Magnetic needle viscometer for Langmuir monolayers. Langmuir. 2002; 18:2800–6.

4. Alonso C, Alig T, Yoon J, Bringezu F, Warriner H, Zasadzinski JA. More than a monolayer: Relating lung surfactant structure and mechanics to composition. Biophysical Journal. 2004; 87:4188–202. [PubMed: 15454404]

5. Alonso C, Bringezu F, Brezesinski G, Waring AJ, Zasadzinski JA. Modifying calf lung surfactant by hexadecanol. Langmuir. 2005; 21:1028–35. [PubMed: 15667185]

6. Alonso C, Zasadzinski JA. A brief review of the relationship between monolayer viscosity, phase behavior, surface pressure and temperature using a simple monolayer viscometer. Journal of Physical Chemistry B. 2006; 110:22185–91.

7. Lingwood D, Simons K. Lipid rafts as a membrane-organizing principle. Science. 2010; 327:46–50. [PubMed: 20044567]

8. Simons K, Toomre D. Lipid rafts and signal transduction. Nature Reviews Molecular Cell Biology. 2000; 1:31–41. [PubMed: 11413487]

9. Choi SQ, Kim K, Fellows CM, Cao KD, Lin BH, Lee KYC, et al. Influence of Molecular Coherence on Surface Viscosity. Langmuir. 2014; 30:8829–38. [PubMed: 24991992]

10. Choi SQ, Squires TM. Dynamics within surfactant layers. Physics of Fluids. 2010; 22:091113.

11. Choi SY, Steltenkamp S, Pascall AJ, Zasadzinski JA, Squires TM. Active microrheology of phospholipid monolayers: seeing stretching, flowing, yielding and healing. Nature Communications. 2011; 2:312.

12. Kim K, Choi SQ, Squires TM, Zasadzinski JA. Cholesterol nanodomains: their effect on monolayer morphology and dynamics. Proceedings of the National Academy of Sciences USA. 2013; 110:E3054–E60.

13. Kim K, Choi SQ, Zasadzinski JA, Squires TM. Interfacial microrheology of DPPC monolayers at the air-water interface. Soft Matter. 2011; 7:7782–9.

14. Wilke N, Maggio B. The influence of domain crowding on the lateral diffusion of ceramide-enriched domains in a sphingomyelin monolayer. Journal of Physical Chemistry B. 2009; 113:12844–51.

15. Wilke N, Mercado FV, Maggio B. Rheological Properties of a Two Phase LipidMonolayer at the Air/Water Interface: Effect of the Composition of the Mixture. Langmuir. 2010; 26:11050–9. [PubMed: 20380451]

16. Mercado FV, Maggio B, Wilke N. Modulation of the domain topography of biphasic monolayers of stearic acid and dimyristoyl phosphatidylcholine. Chemistry and Physics of Lipids. 2012; 165:232–7. [PubMed: 22274694]

17. Kotula AP, Anna SL. Insoluble layer deposition and dilatational rheology at a microscale spherical cap interface. Soft Matter. 2016; 12:7038–55. [PubMed: 27478885]

18. Caruso B, Mangiarotti A, Wilke N. Stiffness of Lipid Monolayers with Phase Coexistence. Langmuir. 2013; 29:10807–16. [PubMed: 23906426]

19. Zasadzinski JA, Ding J, Warriner HE, Bringezu F, Waring AJ. The physics and physiology of lung surfactants. Current Opinion in Colloid and Interface Science. 2001; 6:506–13.

20. Clements JA, Avery ME. Lung surfactant and neonatal respiratory distress syndrome. American Journal of Respiratory and Critical Care Medicine. 1998; 157:S59–S66. [PubMed: 9563762]

21. Bleecker JV, Cox PA, Keller SL. Mixing Temperatures of Bilayers Not Simply Related to Thickness Differences between L-o and L-d Phases. Biophysical Journal. 2016; 110:2305–8. [PubMed: 27238286]

22. Honerkamp-Smith AR, Cicuta P, Collins MD, Veatch SL, den Nijs M, Schick M, et al. Line tensions, correlation lengths, and critical exponents in lipid membranes near critical points. Biophysical Journal. 2008; 95:236–46. [PubMed: 18424504]

23. Honerkamp-Smith AR, Veatch SL, Keller SL. An introduction to critical points for biophysicists; observation of compositional heterogeneity in lipid membranes. Biochemica et Biophysica Acta. 2009; 1788:53–63.

24. Keller DJ, McConnell HM, Moy VT. Theory of superstructures in lipid monolayer phase transitions. Journal of Physical Chemistry. 1986; 90:2311–5.

25. Keller SL, Pitcher WHI, Huestis WH, McConnell HM. Red Blood Cell Lipids form Immisible Liquids. Physical Review Letters. 1998; 81:5019–22.

26. Moy VT, Keller DJ, Gaub HE, McConnell HM. Long-range molecular orientational order in monolayer solid domains of phospholipid. Journal of Physical Chemistry. 1986; 90:3198–202.

27. Stottrup BL, Veatch SL, Keller SL. Nonequilibrium behavior in supported lipid membranes containing cholesterol. Biophysical Journal. 2004; 86:2942–50. [PubMed: 15111410]

28. Veatch SL, Keller SL. Organization in lipid membranes containing cholesterol. Physical Review Letters. 2002; 89:268101. [PubMed: 12484857]

29. Veatch SL, Keller SL. Separation of liquid phases in giant vesicles of ternary mixtures of phospholipids and cholesterol. Biophysical Journal. 2003; 85:3074–83. [PubMed: 14581208]

30. Veatch SL, Keller SL. Seeing spots: complex phase behavior in simple membranes. Biochimica et Biophyisca Acta. 2005; 1746:172–85.

31. Baumgart T, Hess ST, Webb WW. Imaging coexisting fluid domains in biomembrane models coupling curvature and line tension. Nature. 2003; 425:821–4. [PubMed: 14574408]

32. Camley BA, Esposito C, Baumgart T, Brown FLH. Lipid Bilayer Domain Fluctuations as a Probe of Membrane Viscosity. Biophysical Journal. 2010; 99:L44–L6. [PubMed: 20858410]

33. Esposito C, Tian A, Melamed S, Johnson C, Tee SY, Baumgart T. Flicker spectroscopy of thermal lipid bilayer domain boundary fluctuations. Biophysical Journal. 2007; 93:3169–81. [PubMed: 17644560]

34. Heinrich MC, Levental I, Gelman H, Janmey PA, Baumgart T. Critical exponents for line tension and dipole density difference from lipid monolayer blundary fluctuations. Journal of Physical Chemistry B. 2008; 112:8063–8.

35. Tian AW, Johnson C, Wang W, Baumgart T. Line tension at fluid membrane domain boundaries measured by micropipette aspiration. Physical Review Letters. 2007; 98:4.

36. von Tscharner V, McConnell HM. An alternative view of phospholipid phase behavior at the air-water interface. Microscope and film balance studies. Biophysical Journal. 1981; 36:409–19. [PubMed: 6895478]

37. Weis RM, McConnell HM. Two-dimensional chiral crystals of phospholipid. Nature. 1984; 310:47–9. [PubMed: 6738702]

38. Weis RM, McConnell HM. Cholesterol stabilizes the crystal-liquid interface in phospholipid monolayers. Journal of Physical Chemistry. 1985; 89:4453–9.

39. $\pi = 72 - \gamma$, or the surface pressure is the difference between the surface tension of a clean water interface, 72 mN/m, and the actual surface tension of the interface, γ. The maximum surface pressure is 72 mN/m, which corresponds to zero surface tension.

40. Schwartz DK, Knobler CM. Direct observations of transitions between condensed Langmuir monolayer phases by polarized fluorescene microscopy. Journal of Physical Chemistry. 1993; 97:8849–51.

41. Nandi N, Vollhardt D. Effect of molecular chirality on the morphology of biomimetic Langmuir monolayers. Chemical Reviews. 2003; 103:4033–75. [PubMed: 14531717]

42. Vollhardt D. Brewster angle microscopy: a preferential method for mesoscopic characterization of monolayers at the air/water interface. Current Opinion in Colloid and Interface Science. 2014; 19:183–97.

43. Fuller GG, Vermant J. Complex Fluid-Fluid Interfaces: Rheology and Structure. Annual Review of Chemical and Biomolecular Engineering. 2012; 33:519–43.

44. Samaniuk JR, Vermant J. Micro and macrorheology at fluid-fluid interfaces. Soft Matter. 2014; 10:7023–33. [PubMed: 24935487]

45. Vandebril S, Franck A, Fuller GG, Moldenaers P, Vermant J. A double wall-ring geometry for interfacial shear rheometry. Rheologica Acta. 2010; 49:131–44.

46. Rosenfeld L, Cerretani C, Leiske DL, Toney MF, Radke CJ, Fuller GG. Structural and Rheological Properties of Meibomian Lipid. Investigative Ophthalmology & Visual Science. 2013; 54:2720–32. [PubMed: 23513065]

47. Alonso C, Waring A, Zasadzinski JA. Keeping lung surfactant where it belongs: Protein regulation of two-dimensional viscosity. Biophysical Journal. 2005; 89:266–73. [PubMed: 15833995]

48. Dihydrocholesterol, or cholestanol is a saturated variant of cholesterol that is used to minimize oxidation, but is otherwise very similar in its properties to cholesterol.

49. Brady JF. The rheological behavior of concentrated colloidal dispersions. Journal of Chemical Physics. 1993; 99:567–81.

50. Hinrichsen EL, Feder J, Jossang T. Random packing of disks in two dimensions. Physical Review A. 1990; 41:4199–209.

51. McConnell HM. Structures and Transitions in Lipid Monolayers at the Air-Water-Interface. Annual Review of Physical Chemistry. 1991; 42:171–95.

52. Lin B, Mero M, Graber GJT, Schlossman ML, Viccaro PJ. The liquid surface/interface spectrometer at ChemMatCARS synchrotron facility at the Advanced Photon Source. Physica B. 2003; 336:75–80.

53. Kaganer VM, Mohwald H, Dutta P. Structure and phase transitions in Langmuir monolayers. Reviews of Modern Physics. 1999; 71:779–819.

54. Jensen TR, Balashev K, Bjornholm T, Kjaer K. Novel methods for studying lipids and lipases and their mutual interaction at interfaces. Part II. Surface sensitive synchrotron X-ray scattering. Biochimie. 2001; 83:399–408. [PubMed: 11368847]

55. Choi SQ, Se Gyu J, Pascall AJ, Dimitriou MD, Kang T, Hawker CJ, et al. Synthesis of multifunctional micrometer-sized particles with magnetic, amphiphilic and anisotropic properties. Advanced Materials. 2011; 23:2348–52. [PubMed: 21360773]

56. Hermans E, Saad Bhamla M, Kao P, Fuller GG, Vermant J. Lung surfactants and different contributions to thin film stability. Soft Matter. 2015; 11:8048–57. [PubMed: 26307946]

57. Lee KYC, Gopal A, von Nahmen A, Zasadzinski JA, Majewski J, Smith GS, et al. Influence of palmitic acid and hexadecanol on the phase transition temperature and molecular packing of dipalmitoylphosphatidyl-choline monolayers at the air-water interface. Journal of Chemical Physics. 2002; 116:774–83.

58. Ma G, Allen HC. Condensing effect of plamitic acid on DPPC in mixed Langmuir monolayers. Langmuir. 2007; 23:589–97. [PubMed: 17209610]

59. The lift-off pressure is the first deviation from a measured zero surface pressure. The torugh area at the lift-off pressure depends on the amount and concentration of the spreading solution, which is difficult to control exactly. For films of varied composition, this is a way of normalizing the π-A diagrams of monolayers.

60. Vollhardt D, Fainerman VB. Progress in characterization of Langmuir monolayer by consideration of compressibility. Advances in Colloid and Interface Science. 2006; 127:83–97. [PubMed: 17208192]

61. Schwartz DK, Viswanathan R, Garnaes J, Zasadzinski JA. Influence of cations, alkane chain-length and substrate on molecular order of Langmuir-Blodgett films. Journal of the American Chemical Society. 1993; 115:7374–80.

62. Zasadzinski JA, Viswanathan R, Madsen L, Garnaes J, Schwartz DK. Langmuir-Blodgett Films. Science. 1994; 263:1726–33. [PubMed: 8134836]

63. Kitaigorodskii, AL. Organic Chemical Crystallography. New York: Consultant Bureau; 1961.

64. Schwartz DK, Viswanathan R, Zasadzinski JA. Head-tail competition and modulated structures in planar surfactant films. Journal of Chemical Physics. 1994; 101:7161–8.

65. Russel, WB., Saville, DA., Schowalter, WR. Colloidal Dispersions. Cambridge: Cambridge University Press; 1989.

66. Lemaitre J, Troadec JP, Gervois A, Bideau D. Experimental study of densification of disk assemblies. Europhysics Letters. 1991; 14:77–83.

67. Ghazvini S, Ricke B, Zasadzinski JA, Dhar P. Monitoring phases and phase transitions in phosphatidylethanolamine monolayers using active interfacial microrheology. Soft Matter. 2015; 11:3313–21. [PubMed: 25782993]

68. Brooks CF, Fuller GG, Frank CW, Robertson CR. An interfacial stress rheometer to study rheological transitions in monolayers at the air-water interface. Langmuir. 1999; 15:2450–9.

69. Fitzgibbon S, Shaqfeh ESG, Fuller GG, Walker TW. Scaling analysis and mathematical theory of the interfacial stress rheometer. Journal of Rheology. 2014; 58:999–1038.

70. Alonso C, Zasadzinski JA. Linear dependence of surface drag on surface viscosity. Physical Review E. 2004; 69:0216021–6.

71. Reynaert S, Brooks CF, Moldenaers P, Vermant J, Fuller GG. Analysis of the magnetic rod interfacial stress rheometer. Journal of Rheology. 2008; 52:261–85.

Author Manuscript
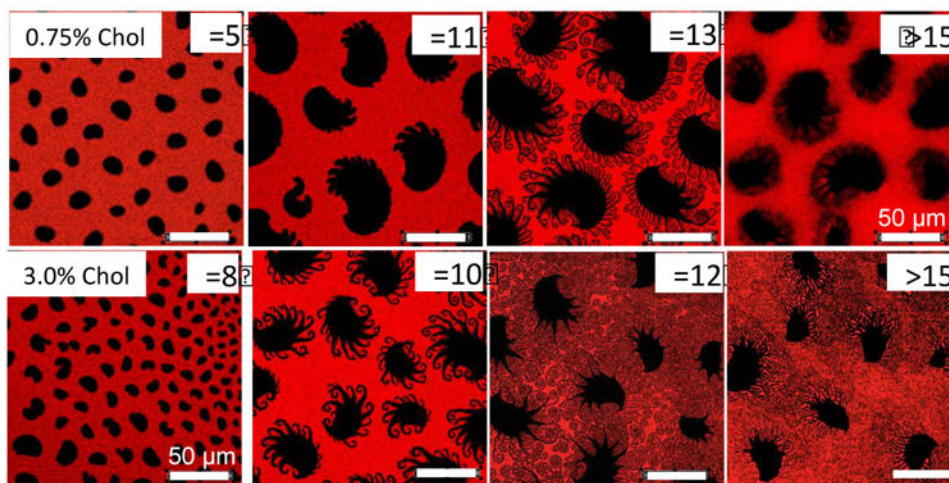
Author Manuscript

Author Manuscript

Author Manuscript

Fig. 1.

Confocal fluorescence images of domain evolution with surface pressure in 3:1 DPPC:PA films with 0.75 or 3 mol% cholesterol. Below 11 mN/m, the monolayer morphology shows round, black, tilted condensed (TC) domains in a continuous red, disordered liquid expanded (LE) phase. Spiral arms nucleate from the domains at $\pi = 11 - 12$ mN/m and fill the space between the solid phase domains as π increases; the spiral arms become so closely packed that they cannot be resolved at higher surface pressure. For $\pi > 15$ mN/m, the black area fraction saturates at a limiting area fraction, A_L.
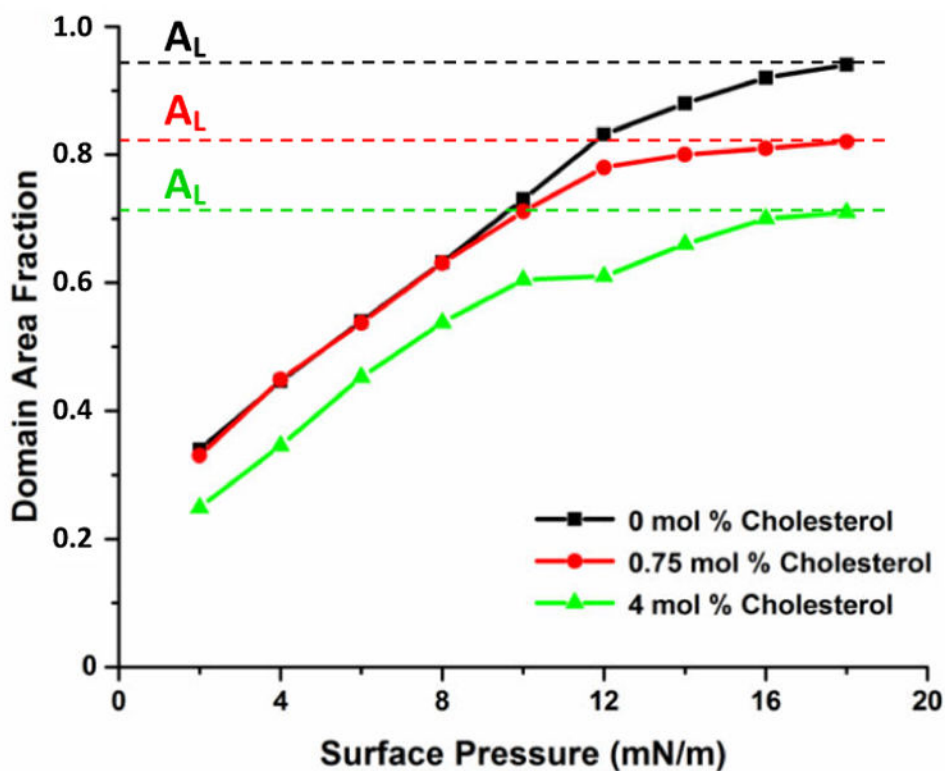
Fig. 2.
Black domain area fraction (From images such as in Fig. 1) as a function of surface pressure for 3:1 DPPC:PA monolayers at different dihydrocholesterol mole fractions. The fraction of black domains increases linearly, then saturates above $\pi \sim 12$ mN/m at alimiting area, A_L, given by the dotted lines. Data is averaged from at least 5 images from 3 independent samples.
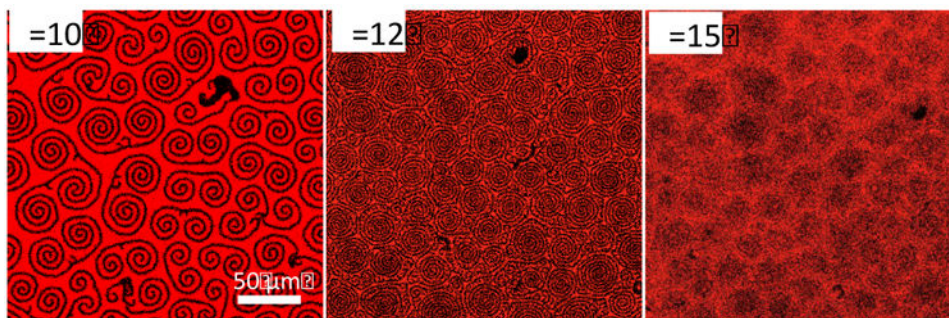
Fig. 3.
Confocal fluorescence images of binary mixtures of DPPC and 2 mol% dihydrocholesterol as a comparison to the morphology of the continuous, red phase in Fig. 1. Dark, spiral arms nucleate out of the LE phase at ~ 10 mN/m and grow and elongate as the surface pressure is increased, as in the continuous red regions of Fig. 1 at higher surface pressure. As the surface pressure is increased, the arms spiral closer and grow together and cannot be resolved, as in the continuous phase in Fig. 1. The similarities in morphology suggests that the spiral arms in Fig.1 growing from the black domains are a second tilted liquid condensed phase of DPPC and dihydrocholesterol.
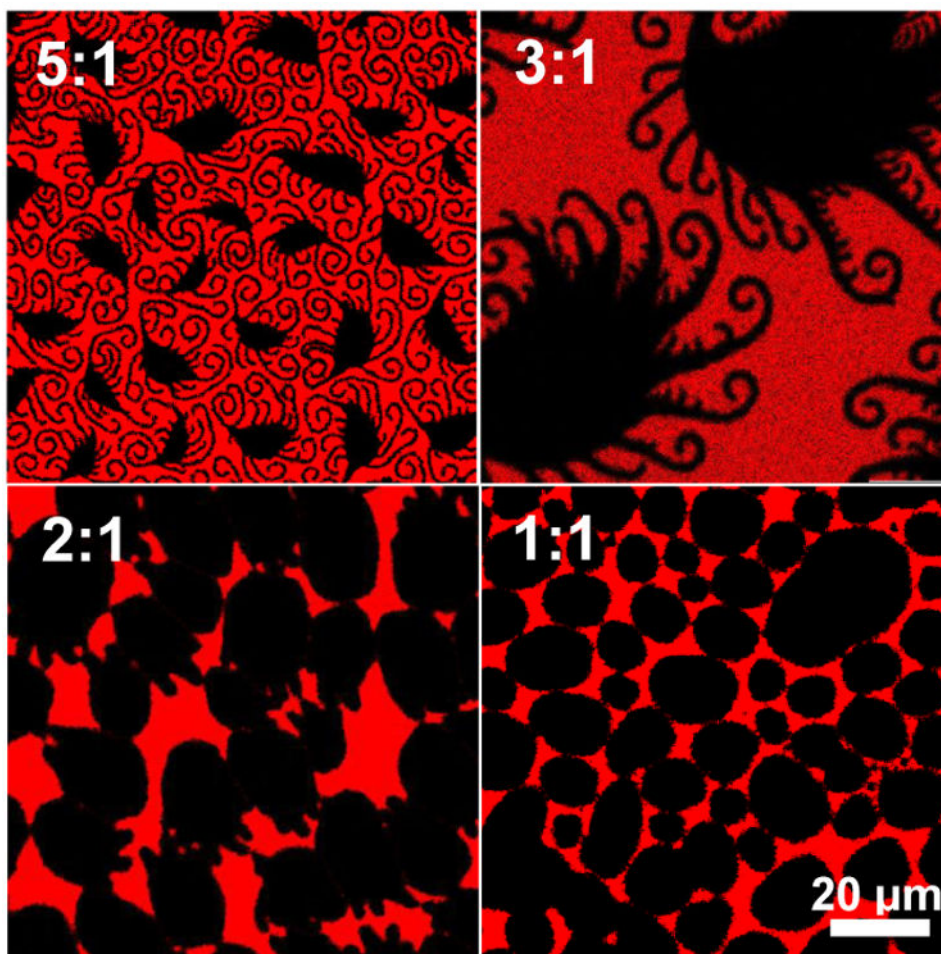
Fig. 4.
Mixtures of DPPC and PA at different molar ratios, with 4 mol% cholesterol at π=11 mN/m. For DPPC:PA ratios of 2:1, 3:1 and 5:1, spiral or straight protrusions extend from the black domains, and the fraction of solid phase decreases with decreasing DPPC fraction. For a DPPC:PA ratio of 1:1, the domains remain round and have no protrusions. This is consistent with the black domains beingco-crystals having a fixed DPPC:PA stoichiometry for the 5:1, 3:1 and 2:1 DPPC:PA monolayers, with the fluid phase (red) being excess DPPC and cholesterol for DPPC:PA of 2:1 and greater (see Figs. 5, 6).
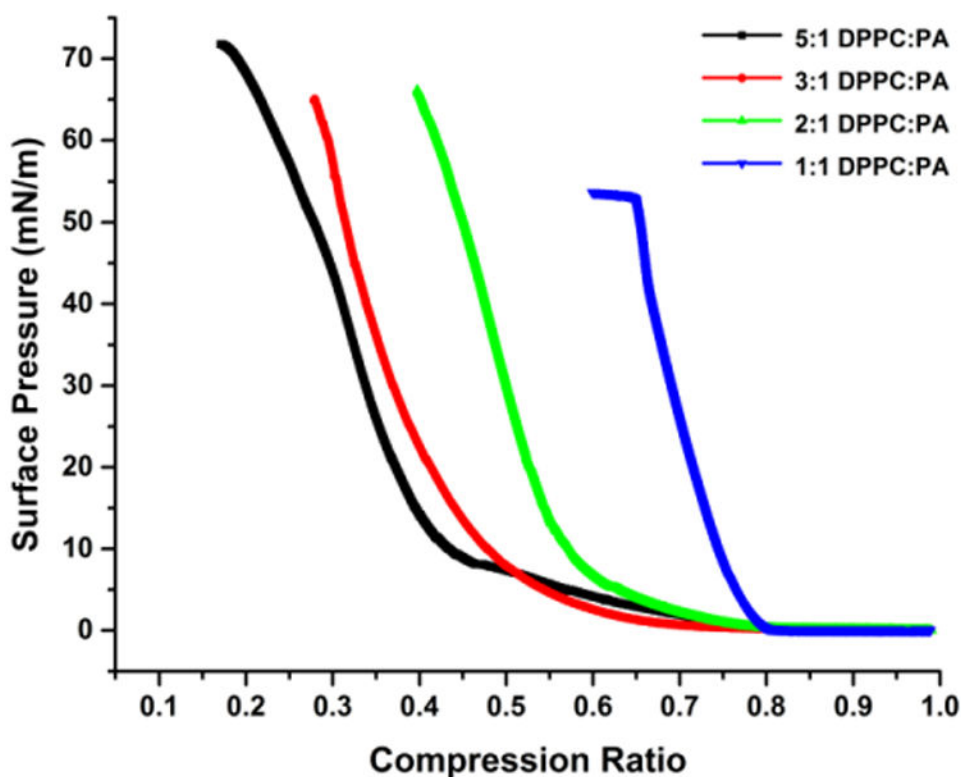
Fig. 5.
Surface pressure- trough area fraction isotherms of 5:1, 3:1 and 2:1 and 1:1 DPPC:PA with 4 mol% dihydrocholesterol adjusted so that the "lift-off" pressure occurs at a trough area fraction of 0.8. The features and curvature of the 5:1, 3:1 and 2:1 isotherms are similar and have similar maximum surface pressures 65 mN/m. However, the isotherm for the 1:1 film is quite different, with a significantly higher compressibility modulus at low surface pressureand a collapse pressure of ~ 52 mN/m.
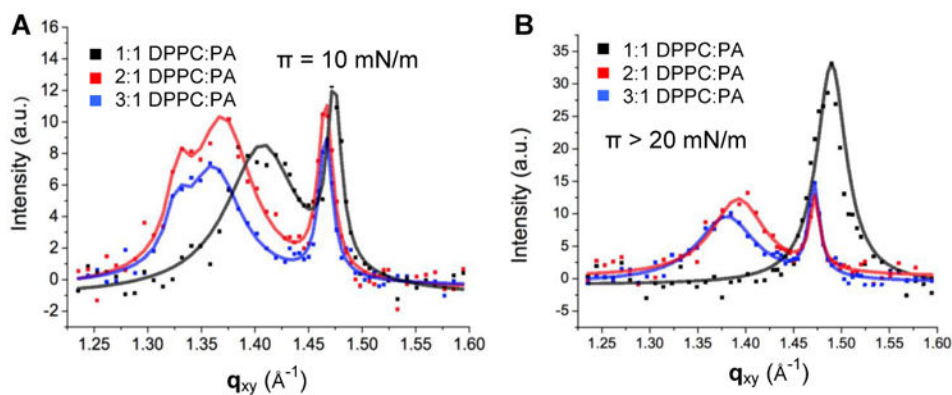
Fig. 6.

A. Grazing Incidence X-ray Diffraction (GIXD) of 3:1, 2:1 and 1:1 DPPC:PA with 4 mol% dihydrocholesterol at 10 mN/m (before nucleation of spiral arms in Fig. 1). All three GIXD patterns have two peaks consistent with a tilted, distorted hexagonal molecular packing, but the low *q* peaks (corresponding to the degenerate (11) direction) of the 2:1 and 3:1 DPPC:PA samples roughly coincide, while the 1:1 DPPC:PA peak is at higher *q*.

B. GIXD of 3:1, 2:1 and 1:1 DPPC:PA with 4 mol% dihydrocholesterolat surface pressures >20 mN/m (after complete transformation of the continuous phase to a spiral arm texture in Fig. 1). The 3:1 and 2:1 DPPC:PA peaks still coincide with each other, and retain the tilted, distorted hexagonal molecular packing. However, the 1:1 DPPC:PA has only a single peak, suggesting an untilted hexagonal packing.
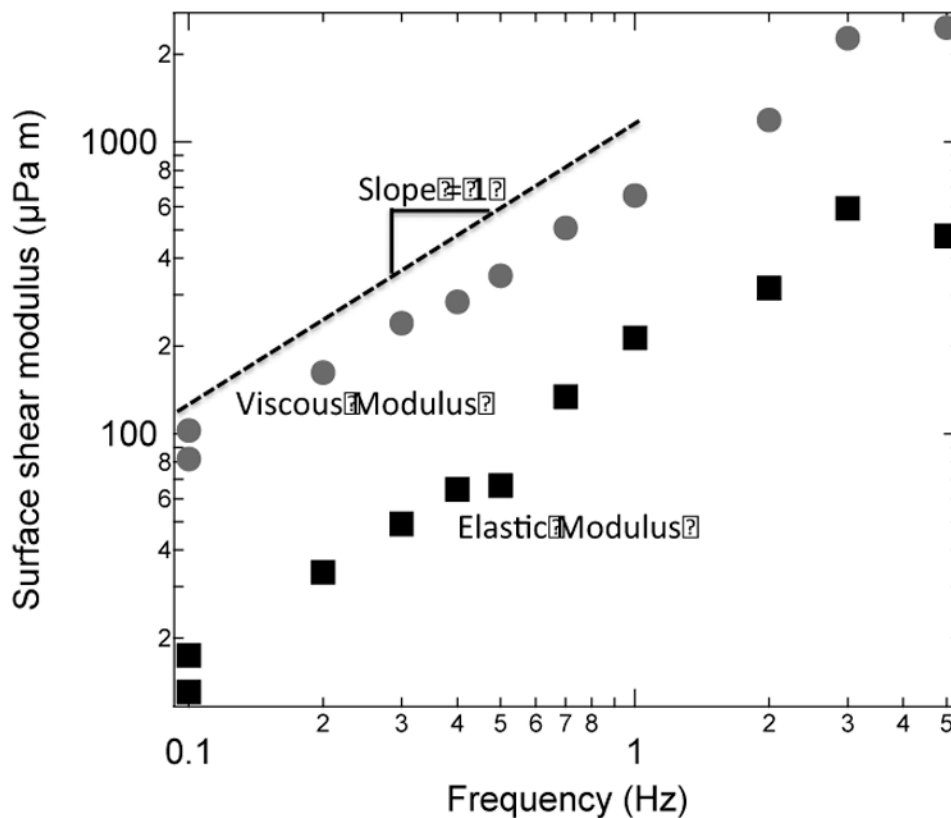
Fig. 7.

Viscous, G_s'' (gray circles) and elastic G_s' (black squares) moduli for 3:1 DPPC:PA monolayer with 1 mol% cholesterol at 15 mN/m as a function of frequency. The viscous modulus is about 10 times larger than the elastic modulus, consistent with a Newtonian film dominated by the surface viscosity. The slope of is G_s'' 1 giving a constant viscosity over the frequency range of 0.1 - 4 Hz within experimental error: $\eta_s = G_s''/2\pi\omega$. Our device cannot reliably measure $G_s'' > 2000$ µPa-s-m; at 5 Hz, the measurements of G_s'' are affected by this limitation.
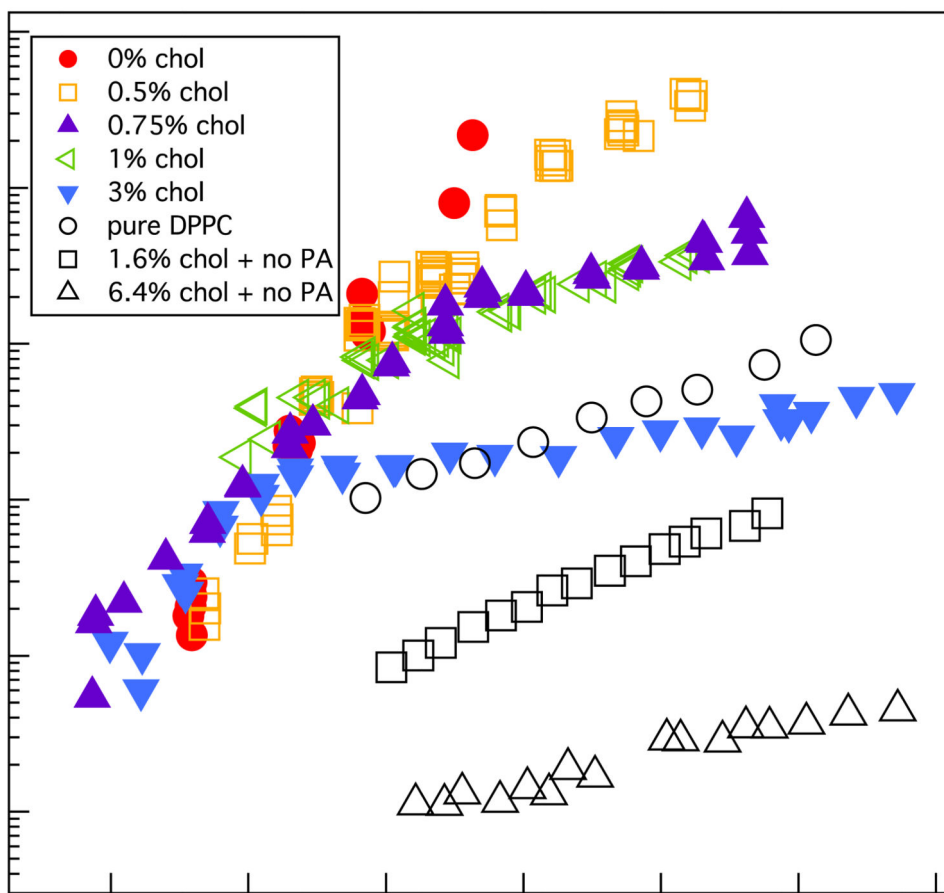
Fig. 8.
Surface shear viscosity of ternary 3:1 DPPC:PA monolayers with different mole fractions of dihydrocholesterol (colored symbols). At low surface pressures, the viscosity increases exponentially with surface pressure, independently of the cholesterol fraction. For surface pressures   12 mN/m, we see an abrupt change of slope and the viscosity decreases by orders of magnitude with increasing cholesterol fraction. The shear viscosity of binary DPPC (no PA) monolayers with 0, 1.6, and 6.4 mol% cholesterol are also presented (open, black symbols); the slopes of these data are similar to that of the DPPC:PA:Chol data for surface pressures > 15 mN/m and show similar decreases with increasing cholesterol fraction.
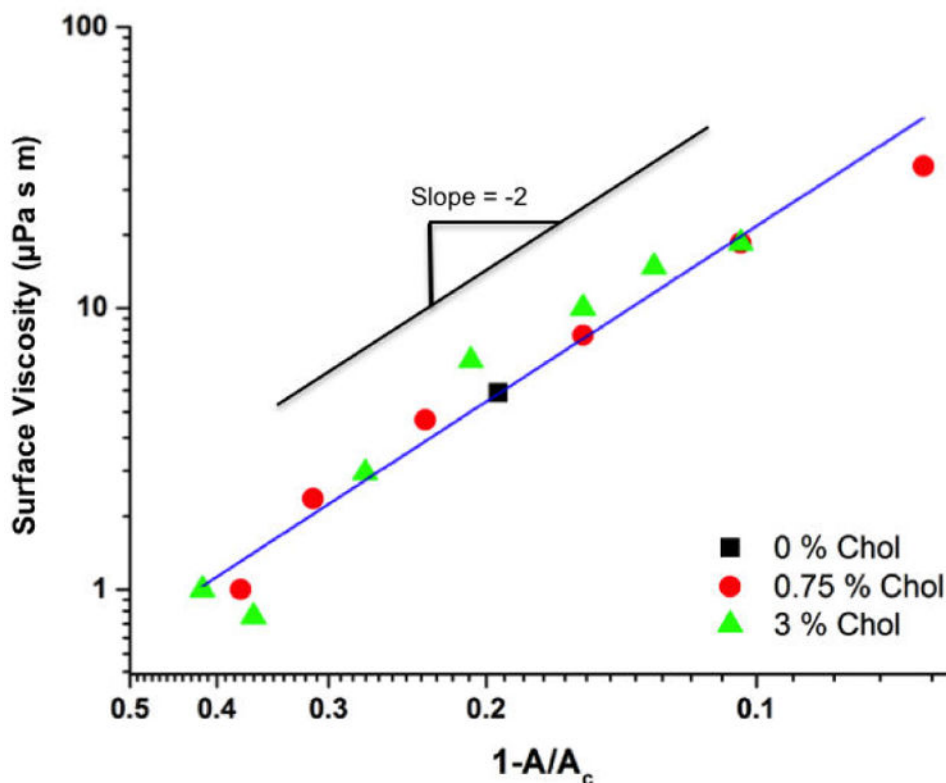
Fig.9.

Fit of surface viscosity data (Fig. 8) to the 2-D suspension model, Eqn. 2, for 3:1 DPPC:PA with varied amounts of dihydrocholesterol for $\pi < 12$ mN/m. Linear regression gives a slope of -2.07 ± 0.13 in agreement with model predictions. The intercept at A=0 gives a constant value for the effective surface viscosity of the continuous matrix $\eta_{so} = 0.16 \pm .03$ µPa-s-m. This low value for η_{so} is consistent with the matrix being in the low viscosity liquid expanded phase; the effective surface viscosity is determined primarily by the drag from the water subphase. The Pearson's r value of the fit to the 2-D suspension model for the data in Fig. 9 is - 0.98, which gives p <0.00001 for the 14 independent data points in the graph.

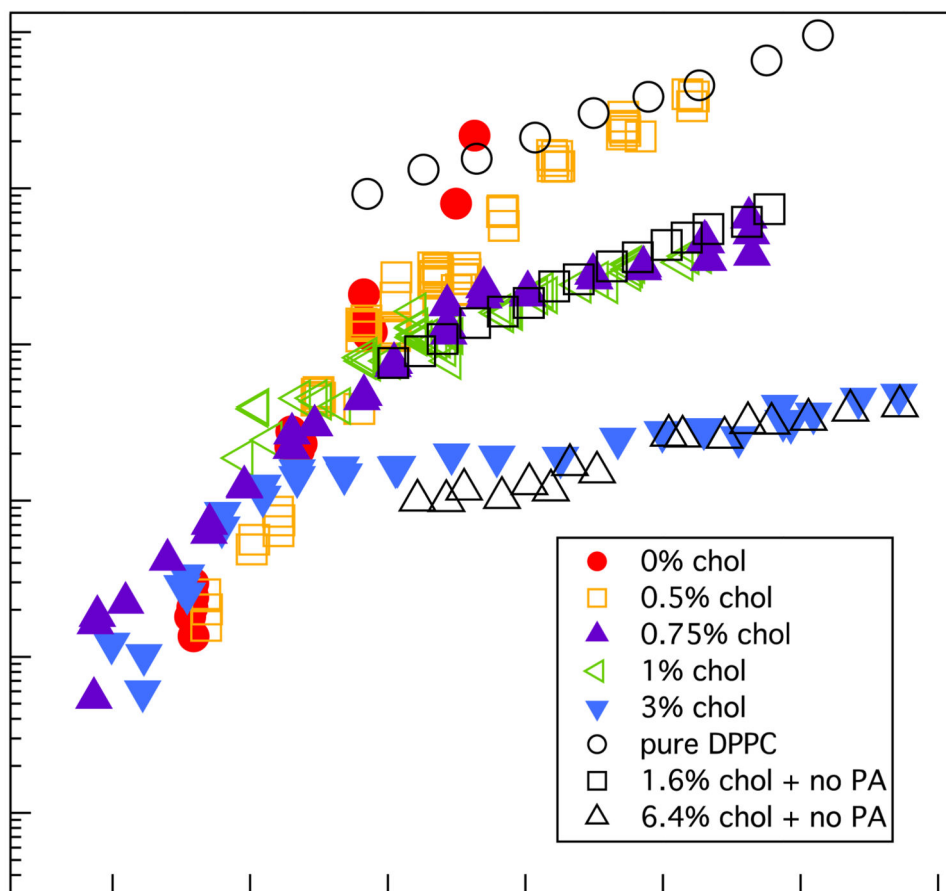**Figure 10.**
The constant η_{so} of the LE phase for $\pi < 12$ mN/m in Fig. 9 is replaced by a variable $\eta_{so}(x, \pi)$ that depends on the cholesterol fraction, x, and surface pressure for $\pi > 12$ mN/m. The 2-D suspension model predicts that for a given area fraction, A_L, log η_{s2} -log η_{s1} =log η_{so} (x_2,π) - log η_{so} (x_1,π), or the differences between the colored symbols should equal the differences between the black symbols for the appropriate value of x. We offset the black symbols according to this equation and the overlap is excellent. The results are consistent with a continuous phase being a binary mixture of DPPC and dihydrocholesterol enriched by a factor of ~ 2 in dihydrocholesterol relative to the nominal concentration.